ISSN 2070-2051, Protection of Metals and Physical Chemistry of Surfaces, 2011, Vol. 47, No. 7, pp. 879–883. © Pleiades Publishing, Ltd., 2011.
Original Russian Text © S.M. Reshetnikov, E.V. Kharanzhevskiy, M.D. Krivilyov, E.Ye. Sadiokov, published in Korroziya: Materialy, Zashchita, 2010, No. 9, pp. 33–37.

PROTECTIVE COATINGS

Corrosion-Electrochemical Behavior of Iron-Based Composite Layers Obtained by Laser Sintering

S. M. Reshetnikov*, E. V. Kharanzhevskiy, M. D. Krivilyov, and E. Ye. Sadiokov
Udmurt State University, Izhevsk, Russia
**e-mail: smr41@mail.ru*

Received May 13, 2010

Abstract—The corrosion-electrochemical behavior of composite layers obtained by high-speed laser sintering of Fe–C ultrafine powders (C in the amount of 0.5 ± 0.1 wt %) is studied using a recording of anodic poteniodynamic curves in borate buffer solutions in neutral and weak alkaline mediums. It is demonstrated that these layers formed on the surface of the steel substrate show the capacity for passivation. Variations in the surface composition and properties of the materials that occur in the course of laser sintering are confirmed using X-ray structural and X-ray electron analyses.

Keywords: laser sintering, composite layers, iron, corrosion, passivation
DOI: 10.1134/S2070205111070148

INTRODUCTION

It is well known, that the corrosive and electrochemical properties of metals and alloys are determined mainly by the state, composition, and properties of surface layers, as well as by the surface microstructure [1–4]. Mechanical stresses, the thermochemical treatment of metals and alloys, and the formation of nonequilibrium structures on their surface often result in an increase in the adsorption activity of the materials, as well as an increase in their anticorrosion properties due to the facilitation of the transformation to the passive state [3–5].

Recently, it was demonstrated [6, 7] that an increase in the dispersity of metals and alloys, including the formation of nanocrystalline phases, results in an increase in the corrosion resistance of composite materials based on iron and its oxides and carbides.

One approach to obtaining nanosized structures on the surface of metals and alloys consists of their laser treatment [8–10]. Taking into consideration the aforementioned, this project was performed in order to investigate the influence of the laser treatment of iron-based metal materials on their corrosion-electrochemical properties.

EXPERIMENTAL

Preparation of specimens. Steel 40 substrate was coated with the composition consisted of mixture of carbonyl iron with addition of 0.5 wt % carbon in the form of graphite. The applied mixture of powdered substances was a pastelike coating, where carbon tetrachloride was used as a binder. The coating was applied to the substrate surface by a roller and the coating thickness was 0.07 mm.

The obtained layer was processed by a fiberoptic ytterbium pulse laser with an emission wavelength of ~1 μm at an emission power density of $\sim 10^8$ W/cm^2. The scanning rate of laser beam in the region of processing equaled 10 cm/s at a pulse frequency of 33 kHz. The processing was performed in an argon protective atmosphere. After the laser processing, the thickness of one sintered layer was 0.05 mm. The process of coating forming and laser processing was repeated several times (up to 16) to achieve the preset thickness of the sintered layer. The purpose of the laser sintering was to produce surface coatings with nanostructural properties.

Optimal modes of processing were selected using mathematical simulation by the method of the two-phase zone [11]. This method, which is widely applied in metallurgy, was extended for the case of the highly intensive thermal processing of powders by laser [12]. The computer model developed based on this approach was used for the quantitative analysis of the rates of heating and cooling, the depth of penetration, and the temperature gradients in the processing region. Based on this data, the coarseness of the crystalline structure and the degree of segregation of chemical components in the sintered layer were estimated. The selected modes provided the formation of nanocrystalline structures on the surfaces of materials [13, 14].

After coating by laser sintering, specimens 1–3 were polished to a depth of 0.1 mm to remove the surface roughness. The specimens had different depths of the remaining sintered layer as follows: for specimen 1,

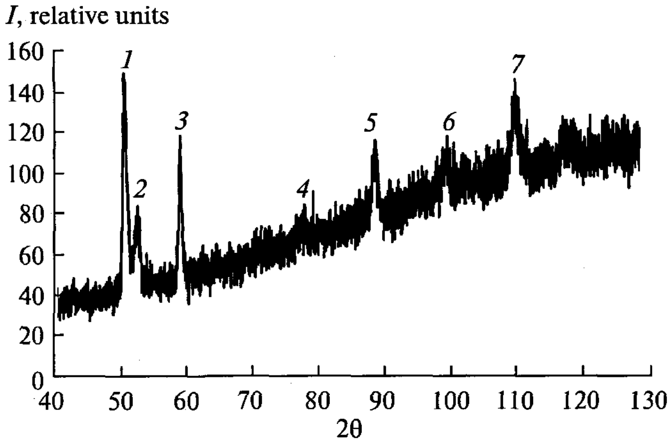

Fig. 1. Diffraction pattern of specimen 3: curves *1*, *3*, *5*, *7*: γ–Fe; curves *2*, *4*, *6*: α–Fe.

it was 0.2 mm; for specimen 2, it was 0.4 mm; and, for specimen 3, it was 0.6 mm. Specimen 4 was not polished after sintering.

Potentiodynamic studies. Polarization measurements of the studied specimens were performed in potentiodynamic mode at a potential scan rate of 1 mV/s using R-30 and IPC-ProL potentiostats and a YaSE-2 cell. The temperature was 22 ± 2°C and the background electrolyte was borate buffer solution with a pH of 7.4–12.4. The aeration of the solution was natural. The selection of this background electrolyte is stipulated by the fact that borate ions are actually indifferent with regard to iron-based electrode materials, i.e., they are not characterized by either the property of their transformation to passive state or by the property to activate, i.e., to disturb the passive state of the surface.

X-ray structural analysis of the specimens was performed using a DRON-6M diffractometer in Co–Kα emission by a constant-time method, gaining intensity in each point by 2θ angle in 5 s. The specimens for the studies using X-ray photoelectron spectroscopy (XPS) were fixed on an indium substrate. At first they were prewashed in rectified alcohol. To study the distribution of elemental concentrations over the depth, etching was performed by argon ions with an energy of 0.9 keV and current density of 12 $\mu A/cm^2$. The etching rate was ~1.0–1.2 nm/min. X-ray photoelectron spectra (XP spectra) of all specimens were obtained at MgKα-excitation (1253.6 eV). Negative pressure in the spectrometer chamber was 10^{-6} Pa. The resolution (width at height half) in the line of $Au4f_{7/2}$ was 1.2 eV. The relative error of the measurement of elemental concentration was 5% of the measured value (in the region of mean concentrations). The accuracy of evalution the bond energy was determined by a scanning step of 0.1 eV.

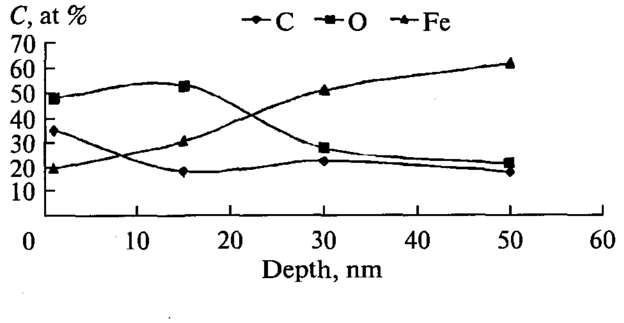

Fig. 2. Profiles of elemental concentrations in depth of sintered specimen 3. Data of XP analysis.

The specimens for electrochemical measurements were in the form of a cylinder with an edge surface area of 0.6 cm^2. The layer formed at the edge of the cylinder served as an electrode operating surface. Inactive electrode surfaces were insulated with epoxy resin.

Prior to electrochemical tests the electrodes were cleaned by fine aluminum oxide applied on wet cloth. Then, the specimens were washed with distilled water and degreased with ethanol, after which the specimens were placed into an electrochemical cell with the appropriate solutions and stored until the stationary potential was achieved (10–15 min), after which the anodic polarization was activated at a rate of 1 mV/s. The potentials were measured relative to the saturated silver chloride electrode. The current density was recalculated with regard to the visible (geometrical) electrode surface. For comparison, polarization curves for Armco iron were obtained under the same conditions.

RESULTS AND DISCUSSION

In the diffraction patterns of the considered specimens 1–4, it is possible to highlight the lines of only two phases, i.e., α–Fe and γ–Fe. Figure 1 illustrates the diffraction pattern of specimen 3 as an example.

Figure 2 illustrates the profiles of elemental concentrations in the depth of sintered specimen 3. It can be seen that oxygen, carbon, and iron exist on the specimen surface. In the course of etching of surface layers the content of two first elements decreases and the iron content increases. Figures 3 and 4 illustrate the X-ray electron spectra of the surface of specimen 3. While the specimen surface contains compounds of iron and oxygen, at a depth of about 30 nm, the predominant portion of iron is in the free state and does not interact with oxygen. At this depth, the ratio of the concentration of iron to oxygen is significantly lower than 1 : 1, i.e., below the homogeneity region of wustite. It is possible to assume that a portion of oxygen is contained in Fe_2O_3 oxide and another portion is in the adsorbed or some other state, which, in terms of the Fe : O ratio, does not correspond to any stoichiometric oxide.

For all specimens, the XP spectrum of oxygen is of at least the two-component type. The component with

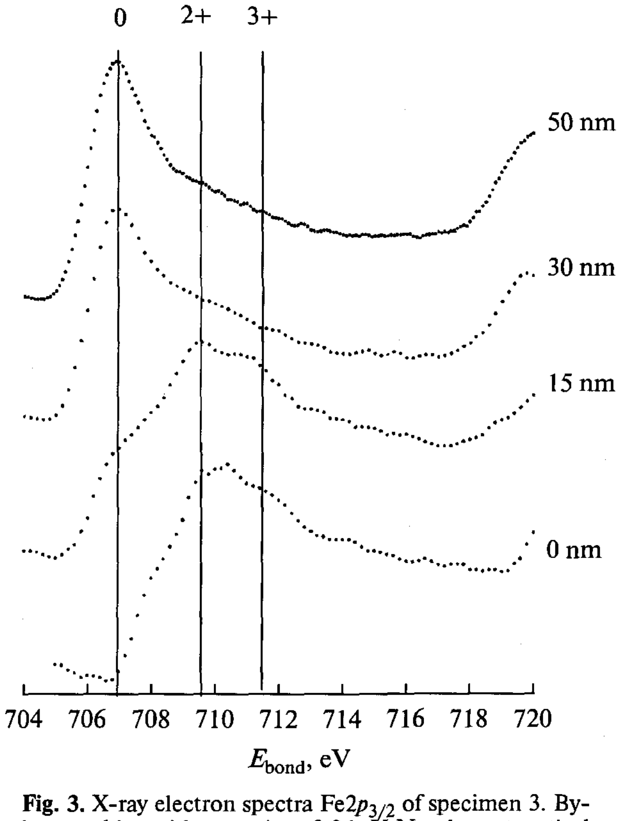

Fig. 3. X-ray electron spectra Fe$2p_{3/2}$ of specimen 3. By-layer etching with argon ions 0.9 keV. Numbers at vertical lines correspond to iron valence state.

E_b = 530 eV corresponds to oxygen bound with Fe (maximum to 0.6 portion of its total content). The second component (all other components) – oxygen in adsorbed state or/and contained in hydroxide groups and bound with carbon (C–O). The XP spectrum of carbon is of an at least three-component type. Here, it is possible to assume that the surface contains carbon in the form of graphite, carbon bound with iron, and carbon with a C–H bond, as well as a C–O bond. Chemical compound C–Fe (cementite) was not observed in the spectra. The majority of carbon is in the C–Fe bond, which corresponds to its solid solution in iron.

Therefore, the surface of the studied specimens obtained by high-speed laser sintering of Fe–C powders consists of complex systems of surface and adsorbed compounds. As mentioned above, the performed mathematical simulation of the development of thermal fields in the laser processing of the powdered layer made it possible to estimate the conditions under which sintering could occur with the possibility of the formation of nanosized structures.

The high speed of heating and cooling (to 10^{11} K/s) during processing by pulse laser emission results in the occurrence of significant (to 10^8 K/m) temperature gradients and a high rate of crystallization, which exerts the main influence on the forming structure.

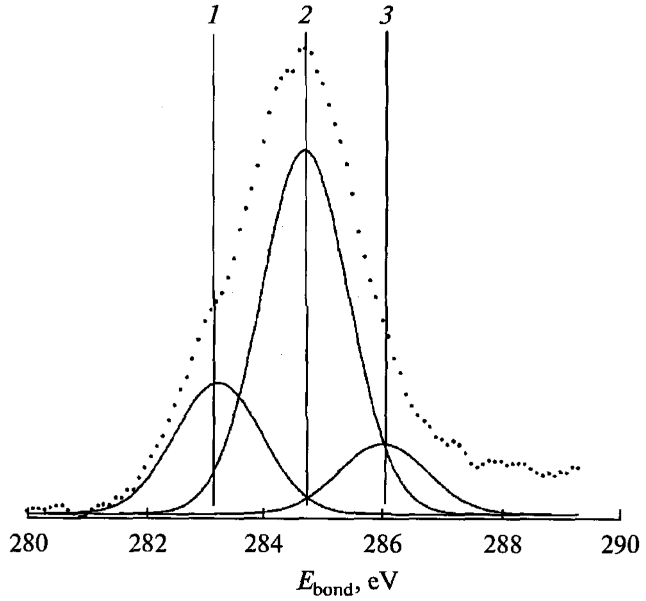

Fig. 4. Decomposition of X-ray electron spectrum C1s of specimen 3 into constituent components. Line *1* corresponds to bond energy C–C, C–Me; line *2* corresponds to bond energy C–H; line *3* corresponds to bond energy C–O.

According to calculations, the maximal speed of the solidification front amounts to 5 m/s. These modes of crystallization result in the suppression of the microsegregation of the components and the achievement of chemically homogeneous structures [13, 14]. An example is given in the table, which presents the results of an X-ray structural analysis of a specimen. It can be seen that the mean size of the crystallites formed during laser sintering is in the range of 10–15 nm.

Figure 5 illustrates the curves of anodic potentiodynamic polarization of Armco iron and specimens 1–3. It can be seen that, under these conditions, all studied specimens are affected by highly pronounced anodic passivation. The rate of anodic ionization of specimens 1–3 in both the region of active dissolution and the region of passivation is significantly lower than that

Results of X-ray structural analysis of specimen1: phase content; lattice parameter *a*; average dimension $\langle L \rangle$ of regions of coherent scattering; relative deformation of crystalline lattice

Phase	Phase content, wt %	*a*, nm	$\langle L \rangle$, nm	ε, %
α-Fe (A2, Body-centered cubic)	37	0.2866	13	<0.1
γ-Fe (0.5 wt % C) (A1, Face-centered cubic)	63	0.3621	15	<0.05

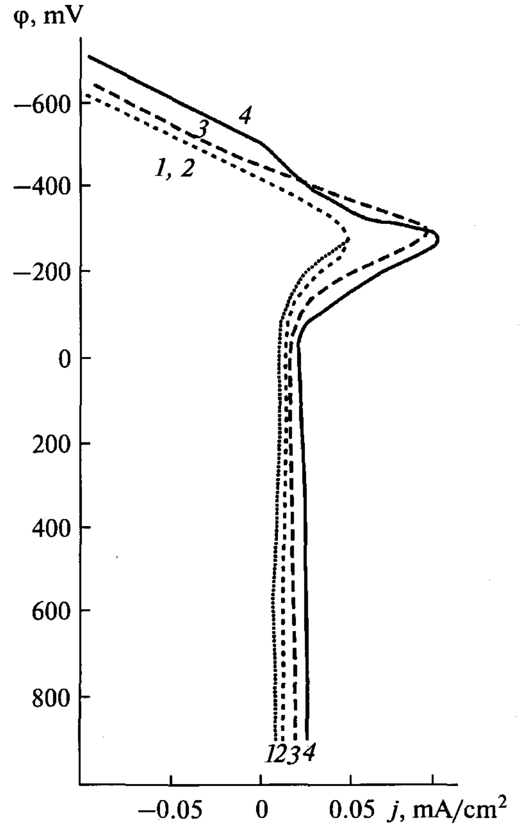

Fig. 5. Curves of anodic polarization of specimens in borate buffer solution at pH 7.4 with sintered on the surface layer Fe—C (0.5 wt %) (curves *1*–*3*) and Armco iron (*4*). The depth of the sintered layer, mm: *1*, 0.2; *2*, 0.4; *3*, *5*, 0.6.

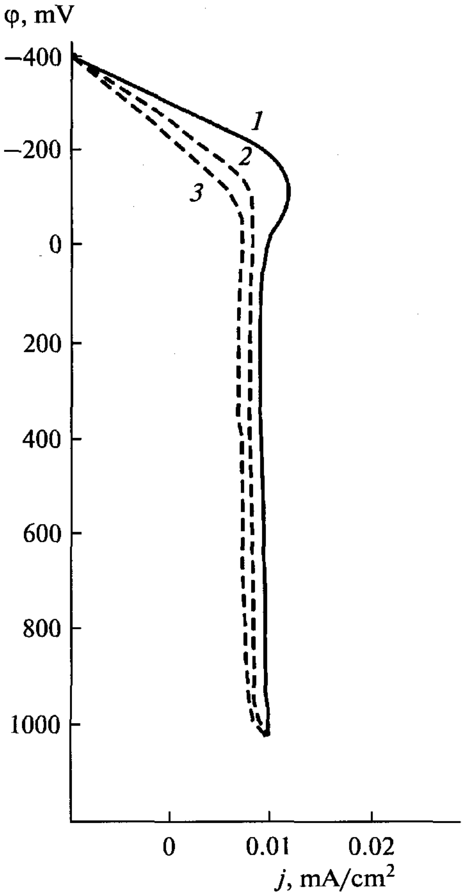

Fig. 6. Curves of anodic polarization of specimen 4 at pH 12.4: *1*, anodic polarization; *2*, reverse course after obtaining of curve *1*; *3*, anodic polarization after obtaining of curve *2*.

of Armco iron. There is no unique dependence between the dissolution rate of specimen and the depth of surface coating. As expected, at an increase in pH, the transformation to passive state is facilitated and, for these conditions, an extremely low velocity of the anodic process is observed (Fig. 6, curve *1* for specimen 4 at pH 12.4).

Therefore, the laser sintering of iron-based powdered materials facilitates passivation process of this material and increases its corrosion resistance. It is known that passive state of iron-based materials is related both with the formation of nonstoichiometric chemosorptive oxide layers, and with formation of hydrate iron oxides [5, 15–20]. Hydrated oxide films formed at the anodic polarization of iron are fairly loose, less dense, and less stable compared to nonhydrated oxides [5]. As mentioned above, after laser processing, the specimens contain surface oxides in nonhydrated form, which provide a lower speed of anodic ionization than the iron on which the hydrated oxide was formed in the course of anodic polarization in aqueous medium.

The lower dissolution rate of the layers obtained by laser sintering in the passive state can be attributed as follows. At increase in anodic polarization, the process of iron oxidation occurs due to existence of defects and pores in the initial passivation layer of Fe_2O_3 and oxide layer of the chemosorptive type. Furthermore, the internal layers of nonoxidized iron under the action of electrolyte that penetrates the pores and defects are oxidized to the state of hydrated oxide, e.g., $Fe(OH)_2$, which closes the pores of free oxide and increases the passivity state, which finally results in a decrease in the anodic current. The process of hydroxide formation is facilitated at an increase in the medium pH, which is confirmed by the comparison of the currents for specimen 3 at pH 7.4 and 12.4.

Let us consider the curves in Fig. 6 as an example that confirms the stability of the passive state of a laser-processed specimen. As was already mentioned, in addition to the phases of α- and γ–Fe, the surface layer of this specimen after laser sintering contains up to 10 at. % nonhydrated oxide Fe_2O_3, which is responsible for the passive state of electrode. Moreover, it can be seen in Fig. 6, that thus phase oxide is highly stable with the consequence that the cathodic polarization at the reverse course of the polarization curve does not result in surface activation, i.e., does not disturb the passive layer containing the Fe_2O_3 phase.

CONCLUSIONS

It is established that the surface layers obtained in the course of the laser sintering of iron-based powders with a carbon content of 0.5 ± 0.1 wt % consist of the phases of α– and γ–Fe and adsorbed and chemically bound oxygen, including in the form of Fe_2O_3. As a consequence, these surface layers obtain the capacity to transform into a stable passive state with increased corrosion resistance in neutral and weak-alkaline mediums.

ACKNOWLEDGMENTS

This work was supported by the Russian Foundation for Basic Research, project no. 09-02-11110-ofi_m, and the Federal Agency for Science and Innovations, project no. 2009-1.5-507.-007-002.

REFERENCES

1. Zhukov, A.P. and Malakhov, A.I., *Osnovy metallovedeniya i teorii korrozii* (Foundations of Metal Science and Corrosion Theory), Moscow: Vysshaya Shkola, 1991.
2. Skorchelletti, V.V., *Teoreticheskie osnovy korrozii metallov* (Theoretical Foundations of Metal Corrosion), Moscow: Khimiya, 1972.
3. Tomashov, N.D. and Chernova, G.P., *Teoriya Korrozii i Korrozionnostoikie Konstruktsionnye Splavy* (Theory of Corrosion and Corrosion-Resistant Structural Alloys), Moscow: Metallurgiya, 1993.
4. Medvedeva, M.L., *Korroziya i zashchita oborudovaniya pri pererabotke nefti i gaza* (Corrosion and Protection of Equipment at Oil and Gs Processing), Moscow: Izd-vo "Neft' i gaz", 2005.
5. Sukhotin, A.M., *Fizicheskaya khimiya passiviruyushchikh plenok na zheleze* (Physical Chemistry of Passivating Films on Iron), Leningrad: Khimiya, 1989.
6. Syugaev, A.V., Lomaeva, S.F., and Reshetnikov S.M., Vliyanie strukturno-fazovogo sostoyaniya nanokompozitov zhelezotsementit na protsessy lokal'noi aktivatsii *Fiziko-khimiya poverkhnosti i zashchita materialov*, 2008, vol. 44, no. 4, pp. 395–399.
7. Lomaeva, S.F., Syugaev, A.V., and Reshetnikov, S.M., Osobennosti anodnogo rastvoreniya nanokompozitov na osnove alpha-Fe-Fe3S v neitral'nykh sredakh, *Korroziya: Zashchita, Materialy*, 2007, no. 1, pp. 2–9.
8. Mirkin, L.I., *Fizicheskie osnovy obrabotki materialov luchami lazera* (Physical Foundations of Metal Processing by Laser Beams), Moscow: Mosk. Gos. Univ., 1975.
9. Kolotyrkin, V.I., Yanov, L.A., and Knyazheva, L.M., Vysokoenergeticheskie sposoby obrabotki poverkhnosti dlya zashchity metallov ot korrozii, in *Korroziya i zashchita ot korrozii. Itogi nauki i tekhniki* (High Energy Methods of Surface Processing for Metal Protection against Corrosion), Moscow: VINITI AN SSSR, 1986, vol. 12, pp. 185–287.
10. Kharanzhevskiy, E.V., Ipatov, A.G., Klimova, I.N., and Strelkov, S.M., Lazernoe spekanie ul'tradispersnykh poroshkovykh materialov na osnove zheleza, *Fiz. Met. Metalloved.*, 2009, vol. 108, no. 5, pp. 534–540.
11. Borisov, V.T., *Teoriya dvukhfaznoi zony metallicheskogo slitka* (Theory of the Two-Phase Zone of a Metallic Ingot), Moscow: Metallurgiya, 1987.
12. Krivilyov, M.D., Gordeev, G.A., Ankudinov, V.E., and Kharanzhevskiy, E.V., Nestatsionarnyi teploperenos pri fazovykh perekhodakh v poristykh materialakh, *Vestnik Udmurtskogo Un-Ta. Fizika. Khimiya*, 2010, no. 1, pp. 43–54.
13. Haranzhevskiy, E.V., Danilov, D.A., Krivilyov, M.D., and Galenko, P.K., Structure and Mechanical Properties of Structural Steel in Laser Resolidification Processing, *Mater. Sci. Eng., A*, 2004, vol. 375–377, pp. 502–506.
14. Herlach, D., Galenko, P., and Holland-Moritz, D., Metastable Solids From Undercooled Melts. Amsterdam: Elsevier, 2006.
15. Kaesche, H., *Die Korrosion der Metalle*, Berlin: Springer, 1979.
16. Kasparova, O.V., Plaskeev, A.V., and Kolotyrkin, Ya.M., Vliyanie chistoty zheleza na ego korrozionnoe i elektrokhimicheskoe povedenie v kislykh sredakh, *Zashch. Met.*, 1985, vol. 21, no. 3, pp. 339–345.
17. Reformatskaya, I.I., Rodionova, I.G., and Beilin, Yu.A., Rol' nemetallicheskikh vklyuchenii i mikrostruktury v protsesse lokal'noi korrozii uglerodistykh stalei, *Zashch. Met.*, 2004, vol. 40, no. 5, pp. 498–504.
18. Reformatskaya, I.I. and Sul'zhenko, A.N., Vliyanie khimicheskogo i fazovogo sostava zheleza na ego pitingostoikost' i passiviruemost', *Zashch. Met.*, 1998, vol. 43, no. 5, pp. 503–506.
19. Corrosion. Edited by L.L. Shreir. City of London. Politechnic, 1963.
20. Todt, F., *Korrosion und Korrosionsschutz*, Berlin: Walter De Gruyter, 1961.